SANDIA REPORT
SAND98–2522
Unlimited Release
Printed November 1998

Recognizing Atoms in Atomically Engineered Nanostructures: An Interdisciplinary Approach

K. M. Horn, G. C. Osbourn, J. W. Bartholomew, B. S. Swartzentruber, A. Bouchard

Prepared by
Sandia National Laboratories
Albuquerque, New Mexico 87185 and Livermore, California 94550

Sandia is a multiprogram laboratory operated by Sandia Corporation, a Lockheed Martin Company, for the United States Department of Energy under Contract DE-AC04-94AL85000.

Sandia National Laboratories

Issued by Sandia National Laboratories, operated for the United States Department of Energy by Sandia Corporation.

Available to DOE and DOE contractors from
Office of Scientific and Technical Information
P.O. Box 62
Oak Ridge, TN 37831

Prices available from (615) 576-8401, FTS 626-8401

Available to the public from
National Technical Information Service
U.S. Department of Commerce
5285 Port Royal Rd
Springfield, VA 22161

NTIS price codes
Printed copy: A03
Microfiche copy: A01

SAND98-2522
Unlimited Release
November 1998

Recognizing Atoms in Atomically Engineered Nanostructures: An Interdisciplinary Approach

K.M.Horn
Radiation Effects Experimentation

G.C.Osbourn, and J.W.Bartholomew
Vision Science, Pattern Recognition, and Multisensor Algorithms

B.S.Swartzentruber
Surface and Interface Science

A. Bouchard
Security Technology Department

Sandia National Laboratories
P. O. Box 5800
Albuquerque, NM, USA 87185-1167

Abstract

This report describes the results of a Sandia Laboratory Directed Research & Development project to develop a technique that can identify atoms in atomically engineered nanostructures. The report provides a detailed description of the experimental measurement techniques and subsequent image analysis procedures used in the identification process, followed by examples of the technique's successful application to several atomic surface features. Use of this technique requires the experimental measurement of both constant-current topographic and multi-bias conductance data from an atomic surface with the scanning tunneling microscope. These measurements are rendered as a collection of topographic and single-bias conductance images of the surface. Image pixels are then grouped into classes by a computed grouping algorithm, according to the shared conductance characteristics exhibited at each pixel. The image pixels are then color-coded by class to produce a false-color image of the scanned surface that chemically distinguishes surface electronic features over the entire area of the measured atomic surface.

A. Introduction

Scanning Tunneling Microscopy (STM) is routinely used to image the electronic wavefunctions of atomic surfaces. Individual features are routinely characterized spectroscopically by measuring current-voltage (IV) spectra [1], conductance (dI/dV) spectra [2], or normalized conductance (dI/dV)/(I/V) spectra [3]. But the chemical identification of surface electronic structures over an entire scanned image has not generally been routinely performed, nor to our knowledge even actively pursued, due to the imposing task of data reduction this entails, and perhaps a belief that suitably unique and reproducible conductance features cannot be obtained.

In the simplest case, in order to determine whether two locations on an atomic surface possess the same electronic structure, one would directly compare the measured bias-dependent conductance spectra from each site. As additional sites were considered, the spectrum from each new site would be compared to those of all previously measured sites. But, even dismissing the sizable task of comparing the conductance spectra of each and every pair of pixels in an image, variations will exist in the spectra of similar sites due to slight differences in neighboring atoms, experimental noise in measuring each conductance spectrum, the presence of sites that are in transition regions from one electronic structure to another, etc. What is needed is a well-defined, yet justifiably flexible definition of the properties of the "conductance signature" for a given chemical species. Such a flexible definition is attained by examining the spatial relationships between the image pixels in an n-dimensional, mathematical space whose axes are the measured tunneling conductance for specific tip-sample biases. The image pixels are plotted in this space according to their measured conductance characteristics and then grouped into clusters, or classes, of similar conductance. The grouping of the data points into distinct classes can be automated through application of a vision science grouping algorithm. The volume of each class distribution in this mathematical space then defines a range of tunneling conductance values at each bias that identify the class. This approach permits variations to exist in the *exact* structure of each pixel's conductance spectrum, while still requiring that the grouped conductance spectra be more similar to each other than to any other classes of conductance spectra sampled from the atomic surface.

Multivariate image analysis has previously been applied to dual-polarity, constant-current, topographic images by Bouchard, et al. to examine the Ge(111) surface [4]. In this work we use multibias conductance images of the Si(001) surface in order to access the full electronic signature of each feature. We show that surface features which are indistinguishable in a topographic image are resolved in a classed image as separate and distinct electronic structures based upon their individual conductance characteristics.

The first portion of this report describes the experimental technique used to record multibias conductance images from atomic surfaces. An example of such images, measured from an atomic step on the Si(001) surface, is shown in figure 1a. The procedures employed in the multivariate image analysis are then introduced: (1) how an initial set of representative conductance spectra are selected from the multibias data using the topograph as a guide, (2) how a discrete set of biases is chosen to discriminate between the selected conductance spectra, and then used as the defining axes of an n-dimensional, mathematical classification space in which the image pixels are plotted, (3) how the image pixels are then grouped together in this mathematical space, either manually or using an automated grouping algorithm, and finally (4) how the grouped image pixels are rendered again as a classed image in real space. The quality of the resulting classification can be evaluated by comparing the computed grouping of the image pixels in every other possible combination of dimensions for the mathematical classification space.

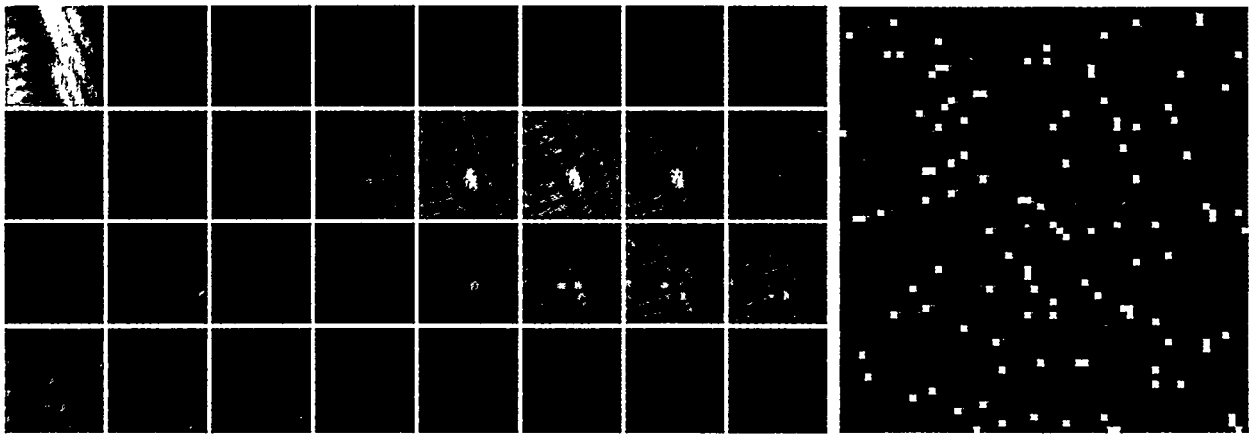

(a) (b)

Fig. 1 (a) Multibias conductivity images of a kink in the A-step of Si(001). The first panel in the upper left is a constant current topograph of the 75x75 Ångstrom scanned region, recorded at -2.5V. The subsequent 31 panels, (from left to right), are conductance images recorded over the voltage range -3V to +3V in steps of approximately 0.2V. (b) The resulting classed image.

B. Measurement of Multispectral STM Images

1. Sample & Tip Preparation

The data shown in figure 1 are from a 75 x 75 Ångstrom scan of a Si(001)-2x1 reconstructed surface. The scan is centered on a kink in a step edge of this 0.25° miscut surface. The 2x1 reconstructed surface consists of dimerized rows of silicon atoms; the dimer bond orientation rotates 90° between adjacent terraces. Consequently, two types of steps exist on the 2x1 surface, one in which the dimer rows on the upper terrace run parallel to the step edge, (termed an A step), and one in which the rows in the upper terrace are perpendicular to the step edge, (a B step) [5]. The scanned area of figure 1 includes both orientations of dimer rows and an A-type step containing a kink.

Before insertion into the STM chamber, the Si(001) sample was swiped with a methanol-dampened cotton swab and blown dry. Once in the chamber, the surface was prepared by two 20 second, ~1250 °C anneals with a chamber pressure of no greater than 1.3×10^{-10} Torr during the anneals. The chamber pressure during the multibias STM measurements was always less than 4.0×10^{-11} Torr.

It has been pointed out by Feenstra, et.al., [6] that relatively blunt tips are found to yield more consistent and reproducible spectroscopic results than much "sharper" tips which exhibit higher spatial resolution. We also find that owing to the requirement of tip stability over frequent and repeated changes of tip polarity and many tens of minutes of continuous measurement for a single multibias conductance image, our best results are obtained with broader tips that easily resolve atomic rows, but do not resolve, for instance, individual dimers along a row. Since the tungsten tip does, at times, contact the silicon sample during initial tip preparation, the presence of silicon atoms on the tunneling tip is very likely. In preparing tips for multibias conductance imaging, we focus primarily on establishing the stability of the atoms at the end of the tip through a series of field emission and tunneling-mode conditioning steps. Though not necessarily the optimum procedure, we outline below the steps we routinely take to prepare a tungsten tip for our multibias conductance imaging measurements.

After an initial tip preparation produces clean topographic images of terrace steps in a 200Å scan, tip stability is checked by retracting the tip to a point where it field emits approximately 10 μA of current at a bias of 200V. Observing the field emission current on an oscilloscope, the tip is left in this condition until 10 minutes elapse with no noticeable transient (i.e. > 0.1 μA) in the emission current trace. If tip instabilities are repeatedly encountered with an otherwise suitable tip, we attempt to 'gently' dislodge the instability by returning to tunneling mode and carefully extending the tip toward the surface until the slightest disturbance in the tunneling current trace is observed. The tip is immediately retracted to the normal tunneling distance. A topographic image is again measured to assure no loss in resolution, and the stability is again checked via field emission. Once the tip proves stable at 10 μA for 10 minutes, the field emission current is lowered to 1 μA and the same procedure is repeated. Once this has also been stable for 10 minutes, we return to the tunneling configuration.

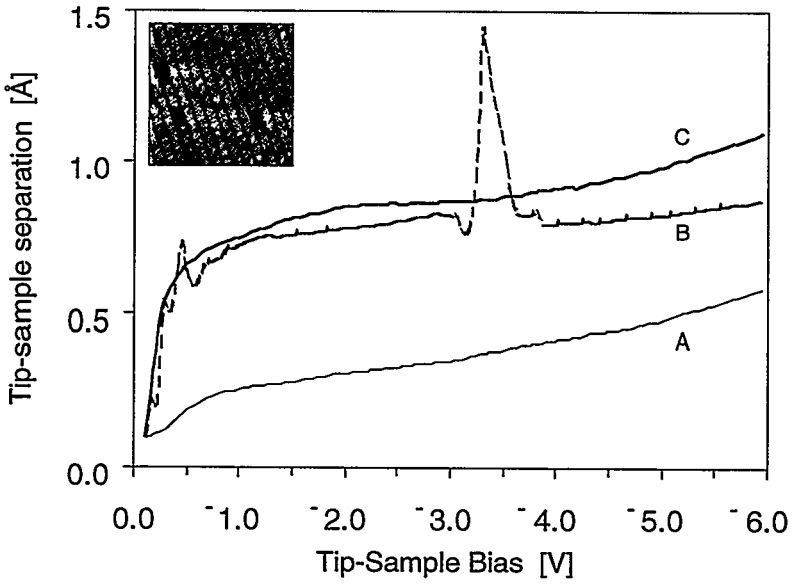

Fig. 2 A plot of the relative tip-sample separation necessary to maintain a fixed tunneling current over a range of tip biases is used to evaluate tip condition. The flatness of curve A indicates a relatively dull tip. It is 'sharpened' through a series of near-approaches to the surface, yielding the steeper slope at low biases shown in curve B. The 'spikes' in curve B, however, indicate the presence of tip instabilities. Continued conditioning of the tip results in curve C, which is stable and produces an image resolution shown in the inset topographic image.

As the last step in tip preparation, we evaluate the tip's condition using a plot of the tip-sample separation necessary to maintain a constant tunneling current (typically 0.1 nA) while the tip bias is ramped over a pre-set voltage range (initially -1.0V to -6.0V); this results in curves such as shown in figure 2. Repeated close-approaches to the surface, (which occur at low biases in this procedure), are found to improve tip resolution. As the tip resolution improves, the slope of the curve at lower biases changes from a flatter response, as in curve A, to a much steeper curve, as in curves B and C. Any tip instabilities induced as the tip bias is changed are observed as spikes in the lineshape, shown in curve B. These instabilities are eliminated either through: 1) continued repetition of the measurement, 2) a near-approach of the tip to the surface, or 3) reverting to the previous field emission step. As the tip stability and sharpness improve, the lower end of the tip bias scan range is gradually reduced, until a final scan range of -0.1V to -6.0V is

achieved. Ultimately, it is upon obtaining a lineshape as displayed in curve C that we find the tip both stable enough for multibias imaging and producing sufficient resolution to obtain a topographic image such as the inset of figure 2.

With this methodology we are able to repeatedly detect unstable atoms on the tip and either force these atoms into some stable site or desorb them, before performing much longer multibias conductance measurements. Though completely empirical, this procedure achieves good results, normally producing multibias images with a day or two of tip preparation.

2. Multibias Conductance Measurement

Multibias conductance images are acquired by measuring the conductance of the tip-sample tunneling junction over a range of biases at each point in a two-dimensional scan of an atomic surface. This measurement technique is distinct from current-imaging tunneling spectroscopy (CITS), in which surface images are measured with a fixed tunneling current at a specific bias by adjusting the tip-sample separation, and then also recording a current-voltage (IV) spectrum at each point. As shown by Stroscio, et al. [7, 8] the image contrast present in CITS images can reflect topographic as well as electronic structure; the effects of topography are greatly reduced in a conductance, (dI/dV), measurement.

The conductance is measured by dithering the applied tip-sample bias while in tunneling range, and

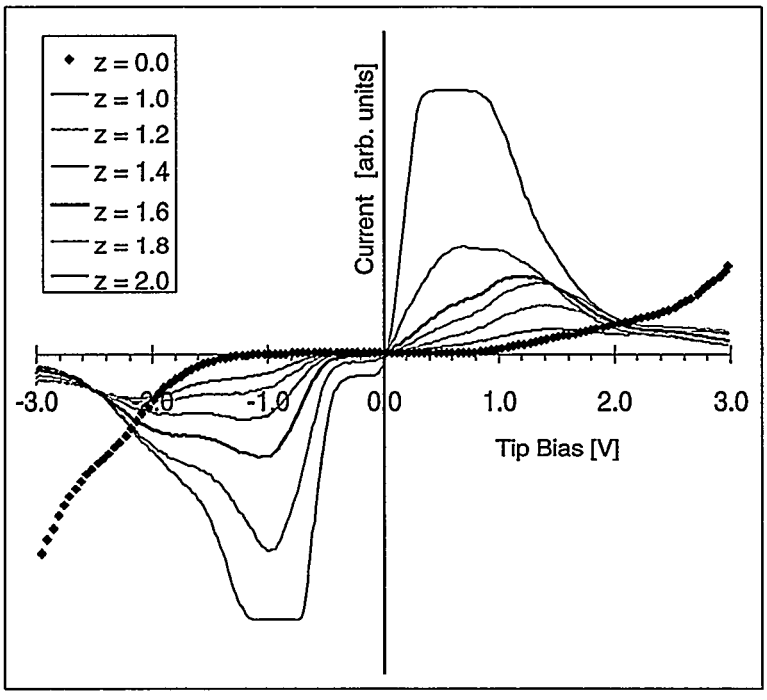

Fig. 3 The effect of varying the tunneling distance as a function of the applied tip-sample bias is shown for IV curves measured using a linear ramp with slopes ranging from z = 0.0 to 2.0

reading the variation in tunneling current at the modulation frequency with a lock-in amplifier. However, conductance measurements at small biases have less sensitivity than those at higher biases, thus masking potentially important electronic features near the band gap. Since the tunneling current is exponentially dependent on both the voltage and the tip-sample separation, the presence of lower tunneling current at

smaller biases can be partially compensated for by employing a variable tunneling distance that decreases the tip-sample separation as the magnitude of the bias is decreased [3, 9, 10]. The slope of this linear compensation is typically between 1.0 and 2.0 Ångstroms/Volt; the selection of the precise value is determined by examining the I/V curves produced over this range of slopes. A selection of I/V curves measured for different slopes is shown in figure 3. An I/V curve measured with no correction applied, (zero slope) is plotted with individual points; a series of I/V curves measured with slopes varying from 1.0 to 2.0 Ångstroms/Volt are plotted as solid lines. Given that this linear correction is somewhat arbitrary, it should be noted that for the purposes of classification, we select the slope which best produces distinguishing features among electronic structures, rather than that which best matches any particular theoretical lineshape. In figure 3, slopes of 2.0 or 1.8 begin to smear out curve features at biases less than 1.0V; thus a slope of 1.6 was chosen for the measurements to be classed below.
In recording a multibias conductance image, the tunneling conductance is measured for each pixel over the full bias range, one point at a time. The sequence of events in the data collection process is: (1) the tip is moved to the first pixel position, (2) the feedback position is read at the pre-selected reference voltage and demanded tunneling current, and recorded for the topographic image, (3) the tip bias is set to the lower bias limit of the conductance measurement range and with a dithered bias ($\approx$ 200mV) on the tip, the measured derivative current signal is averaged over N digitized samplings (typically N=100) and stored in memory, (4) the bias is stepped to the next bias, (5) after a brief settling period (~milliseconds) to accommodate the presence of capacitive coupling between tip and sample, the next derivative current measurement is made. In this fashion, pixel-by-pixel, a sequence of conductance spectra is measured over the entire scanned region. Bias-dependent conductance images are then constructed from these data, as shown in figure 1a.

Since no height-correcting feedback is applied to the tip during the conductance measurements, it is imperative that z-drift be near zero; furthermore, given the longer time duration required to measure, average, and store the derivative current signal over the entire scanned area, it is also important that lateral drift be minimized so that positional registry is maintained among the points in the two dimensional image.

A set of multibias conductance images, measured from an A-step on Si(001), is presented in figure 1a. The first panel in the upper left corner is the topographic image of the scanned area; it was measured in coincidence with the conductance data at a constant current of 0.2 nA for a bias of -2.5V. Subsequent panels (from left to right) display conductance images of the same area recorded over the bias range -3.0V to +3.0 V; each successive conductance image reflects a bias increase of approximately 0.2V. The classed image obtained after performing multivariate image analysis on these experimental data is shown in figure 1b.

The ensemble of conductance images shown in figure 1a contains all the physical information that is used in the image analysis. The multivariate image analysis imposes no physical assumptions onto the conductance data, nor adds any additional data; it merely groups pixels of similar conductance. In simple cases, differing surface features can often be identified directly from the raw conductance images. In the present example, the feature-giving rise to the unique electronic states at the kink in the A-step is seen directly in those conductance images near the band gap. In only slightly more complicated surfaces, the number of biases that must be simultaneously correlated in "the mind's eye" quickly becomes too large for direct identification of many electronically unique features. It is under such conditions that the computed classification is most useful.

C. Classification of Multispectral STM Images

1. Rendering Data in the Classification Space

The physical property that is used as the basis for grouping image pixels into discrete classes is tunneling conductance. The individual steps in the classification process are shown in figure 4. First, conductance spectra are sampled from sites whose similarity is suggested by the topographic image (figure 4a). Each different type of feature is termed a *class* and the points that are selected to represent a class's conductance characteristics are called *training points*. The conductance spectra sampled from each class are overlaid to determine if they are qualitatively similar. Spectra from different classes are contrasted to assure that they are indeed different. The color-coded conductance curves from the training points of the three proposed classes in this example are displayed in figure 4b. Each curve represents the measured tunneling conductance as a function of tip-sample bias over the range -3.0 to +3.0 V.

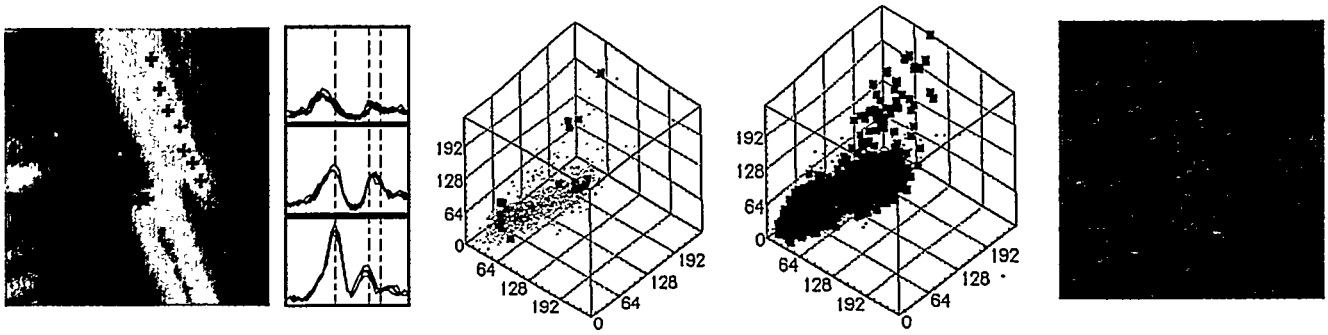

Figure 4. Steps in the classification process: (a) An initial sampling of training points is selected to represent each proposed class. (b) Dimensions are selected which distinguish between the representative conductance curves. (c) A mathematical 'classification' space is constructed in which to group image pixels into classes. (d) Each pixel is grouped, if possible, with one of the proposed classes. (e) The 'classed' pixels are rendered again in real space; black pixels failed to group with any of the proposed training data.

Individual biases are then identified which can be used to distinguish each class's conductance spectrum. These biases are marked with vertical dashed lines in figure 4b. It is sometimes necessary to select three or more biases in order to obtain differences in conductance between all classes in at least one bias. The selected biases are then used as the *dimensions* for a mathematical, classification space, shown in figure 4c. It is within this mathematical space that the image pixels are grouped into classes according to their measured conductance.

Each axis of the classification space represents the tunneling conductance measured at a specific tip-sample bias; measurements at each bias are equalized and scaled from 0 to 255. The mathematical classification space can, in principle, have any number of dimensions. In this example, three dimensions are sufficient to discriminate between the classes. The initial set of color-coded training points are plotted in this space in figure 4c. The remaining pixels in the image, which have not been assigned a class identity, are called *test points*; these are plotted as gray dots in figure 4c.

The process of determining whether each test point groups with one or more training points is termed 'classifying' the image. We have used a computational grouping algorithm to perform this task, yielding the results in classification space shown in figure 4d. (The explicit operation of the grouping algorithm is

explained in further detail below). The grouping of a test point with a training point conveys the class identity of the training point onto the test point. This procedure is the sole means of 'coloring' (i.e. assigning a class identity to) pixels in the classed image. It should be pointed out that the groupings could alternatively be assigned manually if the topology of the point distribution in the classification space is suggestive enough, (i.e. if clusters of points became apparent when plotted in the conductance-based classification space.) However, manual grouping of the data does introduce a greater degree of subjectivity into the classification.

As a final step in the classification, the grouped data are rendered again as a real-space image, as in figure 4e. Each pixel is colored according to the conductance class into which it has grouped; it is colored black if it has not grouped with any existing class, or white if it has grouped with multiple classes. Based upon these results, the class-defining regions of the classification space are then refined in order to try to incorporate the remaining unclassed image pixels into one of the classes and to minimize the number of pixels which have grouped into more than one class. When using the computed grouping algorithm, the boundaries of the class-defining region are governed by the selection of training points; including additional training points, or removing questionable points, permits the class-defining region to be refined. New classes may be created to represent features, which did not group into any of the existing classes. Existing classes can be discarded if found to be not unique. Thus, the initial creation of classes using features suggested by the topograph serves only as a starting point, and decreases in importance as the classification process proceeds. In this iterative manner, features that may appear similar or indistinct from their surroundings in the topographic image are resolved in the classification space and discriminated in the classed image.

In the measurements presented here, the conductance spectra consist of 31 measured biases ranging from -3.0 to +3.0 V. The recorded value for the tunneling conductance at each bias is obtained by averaging 100 individual measurements. In the context of the mathematical classification space, each of the 31 tip-sample biases can be thought of as a separate dimension in which to resolve the conductance spectra associated with each surface feature. It has been demonstrated that the use of the *fewest* possible dimensions actually produces the *best* classification [11]. It is important to emphasize again that the term "dimension" refers to the particular selection of tip-sample biases, which are used to discriminate between the already-measured conductance spectra. The spectra, themselves, are measured with the maximum feasible number of samplings at each bias, (in this example, we averaged 100 conductance measurements at each bias); but the separate, subsequent task of distinguishing between, and grouping, these spectra is found to be optimized by minimizing the number of individual biases used to compare the spectra. The purpose of re-casting the data into a new, mathematical space is to separate it out into resolvable regions. Some minimum number of useful dimensions is clearly needed to separate the distinguishable classes. However, including additional dimensions may not provide further separation of these class volumes, and may in fact add "noise," i.e. the classes may actually move closer to each other in this new space. Thus, minimizing the number of dimensions typically makes the classification procedure more robust against measurement noise and variability of the class spectra.

Any quantifiable feature of the conductance spectra can be used as a dimension. Such properties as the slope of the conductance spectra at a given bias or the intensity gradient of the conductance in a given real-space direction are equally valid dimensions. In this example, the conductance at three specific biases proved sufficient to differentiate between the various spectra. However, dimensions can be changed, deleted or augmented with other discriminating dimensions as the classification results warrant.

2. Grouping Data in the Classification Space

In simple cases where the conductance classes can be distinguished with only a few biases, the grouping of points in classification space can be achieved by human inspection. Though prone to an undesirable

degree of subjectivity, manual grouping can be employed for distributions exhibiting obvious clustering. Whether performed manually or with a computed algorithm, the primary criterion for accepting a pixel's grouping with a specific class is that its class identity is consistent with the class identities of surrounding pixels in both real-space and classification space. Regions of transition from one representative conductance class to another may be reliably left unclassed when these pixels, in a real space image,

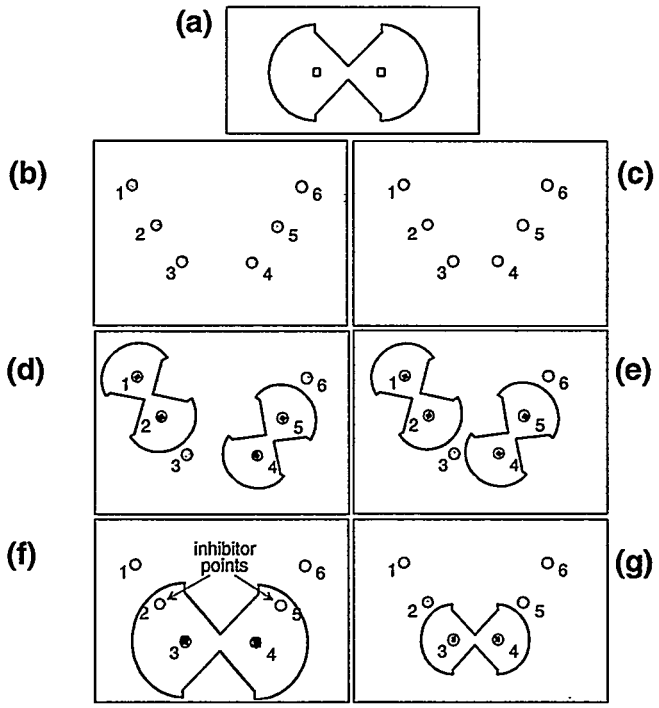

Figure 5. Examples of the use of the VERI-template: Panel (a) shows the VERI template and its two scaling 'foci'. Two different distributions of points to be grouped with the VERI template are shown in panels (b) and (c). In panels (d) and (e) two separate applications of the VERI-template are shown. The template is scaled to the size of separation between two points being tested (points 1 & 2 and 4 & 5, in this example); in both panels both sets of points are seen to group since no other points fall within the scaled VERI-template's boundary. However, in panel (f), when scaled to the separation of points 3 and 4, these points do not group since point 2 (and also 5) fall within the boundary of the VERI template. In panel (g) however, no other point is present within the boundary of the VERI-template, so points 3 and 4 do group. Thus, when applied to each possible pair of points in the distributions shown in panels (f) and (g), the VERI template groups the points in panel (g) as a single class, but finds the distribution of points in panel (f) to be two separate classes - just as the human eye does.

pairs of points exist to be tested.

Since any number of dimensions can be used to distinguish the conductance spectra of each class, the mathematical classification space in which the grouping of image pixels occurs is an n-dimensional hyperspace, where n is the number of dimensions (biases) selected. However, because the VERI template acts only on three points at a time, the relative orientation and separation of any combination of three points in this n-dimensional space is always defined in a plane and the VERI-grouping proceeds as depicted in figure 5 - no matter how numerous the number of descriptive dimensions.

Because the dimensions of the hyperspace correspond to those biases, which discriminate between characteristic features of the sampled conductance spectra, the spectral lineshape associated with each pixel of the real space image can be accurately represented by a single, unclassed, test point in this space. The VERI template can then be applied to determine possible groupings between each unclassed test point (i.e. unknown conductance spectrum) and each classed training point (known conductance spectrum). If grouping is not inhibited by another training point, the test point is assigned the class of the training point it has grouped with. If all groupings of a given test point occur with training data of a single class, the class assignment is to that single class. If no groupings occur between a test point and any existing training data, the test point remains unclassed and is colored black in the real space, classed image. If groupings occur with multiple classes of training data, the class identity of the test point is unclear and the pixel is colored white in the classed image.

Owing to the grouping 'behavior' of the VERI template, pixels that are grouped into a class need not have exactly the same conductance line shape as any other points already in the class. In fact, if added to a class's training data, the newly admitted class point can act to extend the definition of the class volume in the classification space. This "growth" behavior allows iterative applications of the classification algorithm to refine the classed image. In the next iteration, the newly extended class definition may now group yet more pixels into the class. However, a point that has already been grouped with one class will still be tested against every other training point to see if it also groups with other classes. As the definition of a class becomes too encompassing, the effect is immediately visible in the classification result as more and more pixels become multiply-classed. In that case, the training data of the classes is adjusted to eliminate the multiple definition.

As the classification is refined through repeated applications, with successively more accurate and inclusive class training points, the number of image pixels that are multiply-classed or not classed is gradually reduced, until no further improvement is observed. Pixels that group with no defined class, or

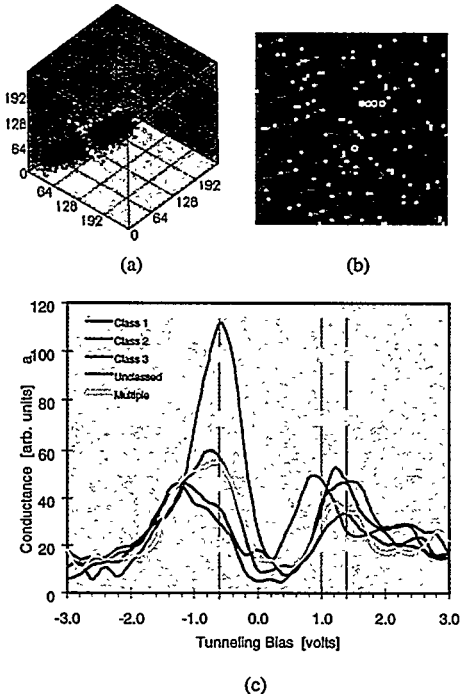

Fig. 6 After successive refinements to the initial training data, a final classed image is produced. (a) The classification space rendering of the final pixel groupings; white pixels have grouped with two or more classes. (b) The real space rendering of the final pixel groupings. (c) Conductance spectra are shown for the classed, unclassed, and multiply classed pixels circled in yellow in the real space image.

with multiple classes, can still occur in the classed images, especially at locations where transitions occur between well-defined electronic states. This is seen in figure 6b where the multiply-classed white pixels and unclassed black pixels all fall at the real-space boundaries between conductance classes representing the rows, troughs, and step edge kink in this dimerized Si(001) surface.
The classification process is an iterative one that depends upon repeated application to produce a classed image that: (1) assigns nearly all the pixels in the image to one of the defined classes, (2) does not contradict the presence of surface features indisputably suggested by the topograph, and (3) produces class volumes in the classification space that are well localized and/or resolved. These features can be seen in the rendering of the classification space and classed real-space image in figure 6a and 6b.

Some measure of the discriminating power of this classification process can be seen in figure 6c, where four conductance curves are plotted from nearly adjacent pixels in the real-space image (circled in yellow in fig. 6b). It is clear that the shapes of the conductance spectra sampled from pixels representing classes 1 and 2, an unclassed pixel, and a multiply classed pixel, are not distinctly unique. Yet the clarity of the overall classed image supports the classification of each.

D. Evaluating the Quality of the Classification Space

In examining the classification with a critical eye, it is important to remember that the training points that initially define the classes are selected from surface features suggested by the topograph; there is no guarantee that these points will form natural clusters when plotted in the classification space. Thus, examination of the positioning of the training points in the classification space is a first check on erroneous class definitions.

The objective grouping of test points with the training points by the computed grouping algorithm serves as a second check on subjective interpretations. However, since the dimensions of the classification space in which these groupings are made, (and in which the VERI template operates), are manually selected by comparing conductance spectra from all classes, the chosen dimensions may not necessarily be the most discriminating ones. The selection of classification space dimensions must therefore also be examined for its validity.

To evaluate the selection of dimensions used to create the classification space, the final sets of training data are themselves grouped in a series of different classification spaces which represent every possible combination of the available dimensions. If the user-selected training data do indeed accurately represent the different classes of conductance present at the surface, and the selected dimensions of the classification space accurately resolve the different conductance spectra, then the VERI template should impartially group the training points together into the same sets of classes as was initially proposed. If the impartial VERI-based grouping does not group a training data point with its user-assigned class, then this is an indication that either the dimensions of this classification space are not resolving the different classes, or that the training point has been incorrectly assigned to represent a class and should not be used as a training point.

Performing such a series of classifications using every possible combination of dimensions is, of course, a computationally intensive undertaking. As such, it is executed on a SunHypersparc workstation with four, 90 MHz processors. For the 64x64 pixel images used in this work, we examined all possible combinations of dimensions in three, four and five-dimensional classification spaces. Including the topographic image as one of the possible dimensions, a total of 4,960 possible combinations exists for a 3-dimensional classification space; 35,960 combinations exist for a 4-dimensional space, and 201,376 different combinations exist for a 5-dimensional classification space. The Sun platform computed the classification results at a rate of approximately 29 combinations/minute/processor. The classifications for all 3-dimension combinations required 43 minutes to compute; all possible combinations in 4-dimensions

required 316 minutes (~5¼ hours), and the 5-dimension combinations required 1,715 minutes (~28½ hours). Comparing the rate of computation for individual processors on PC platforms - a 200 MHz Pentium Pro is approximately 1.5 times as fast, and a 200 MHz Pentium is approximately 0.9 times as fast, as a single processor in the Hypersparc.

The grouping results from each different classification space are collated and used to evaluate how well each selection of dimensions grouped the training data into the pre-assigned classes. For each combination of dimensions, a list is generated which indicates the number of training points which have grouped into either, (a) their original user-assigned class, (b) a single, different class, (c) more than one class, or (d) no class at all. This list is then examined to determine how well the initial selection of dimensions and training data performed, and if there exists a better set of dimensions for classing the experimental data.

In the present classification, the use of the three dimensions 13, 21 and 23 (biases -0.6, +1.0, and +1.4V), produced a result in which a total of 96.8% of the training points grouped with their initial class. Classifications performed in every other combination of three dimensions revealed that a slightly better grouping result could have been attained using dimensions 1, 21, and 25 which would have resulted in an agreement of 98.4% between the grouped training data and their pre-assigned classes. If the number of dimensions used in the classification space is expanded to include four or five dimensions, there exist 176 different combinations of four and five dimension classification spaces which would have done marginally better than *any* three dimension classification, exhibiting 100% agreement between the initial class assignments and the grouping results.

E. Example: A-Step of Si(001) Surface

The Si(001)-2x1 reconstructed surface consists of dimerized rows of silicon atoms; the dimer bond orientation rotates 90° between adjacent terraces. Consequently, two types of steps exist on the 2x1 surface, one in which the dimer rows on the upper terrace run parallel to the step edge, an A-step, and one in which the rows in the upper terrace are perpendicular to the step edge, a B-step [14]. Both images presented in figure 7 cover a 75x75 Å area centered on an A-type step containing a kink. The classed images display the expected periodicity of the dimer row structure in both domains, in agreement with models of the dimerized surface. Three features are common to both images: the dimer row (light gray class), dimer trough (dark gray class), and kink in the A-step (red class). Several other anomalous features also appear in the classed images.

In figure 7a, the topograph contains an irregular feature in the middle of the lower terrace; it lies along the center of a dimer row in this empty states image. In the classed image, however, this defect does not exhibit an electronic structure uniquely different from that of the surrounding dimer trough and row structures. Electronically, it appears simply as a break or gap in the dimer trough (dark gray in the classed image). Thus, although this technique cannot image subsurface causes of surface irregularities, (unless its electronic structure extends to the surface), comparison of the resulting topographic and conductance-based images, (e.g. figure 7a), can reveal whether a given surface irregularity in a topographic image is electronically unique.

An example of a defect which exhibits both topographic and electronic uniqueness is seen adjacent to the kink in figure 7b. Visible both in the topograph and as the cluster of blue pixels in the classed image, the conductance spectrum of this feature is seen to differ markedly from those of the other conductance classes, especially at biases less than -2.0V. In this case, the topographic irregularity does indicate the presence of an associated electronic defect.

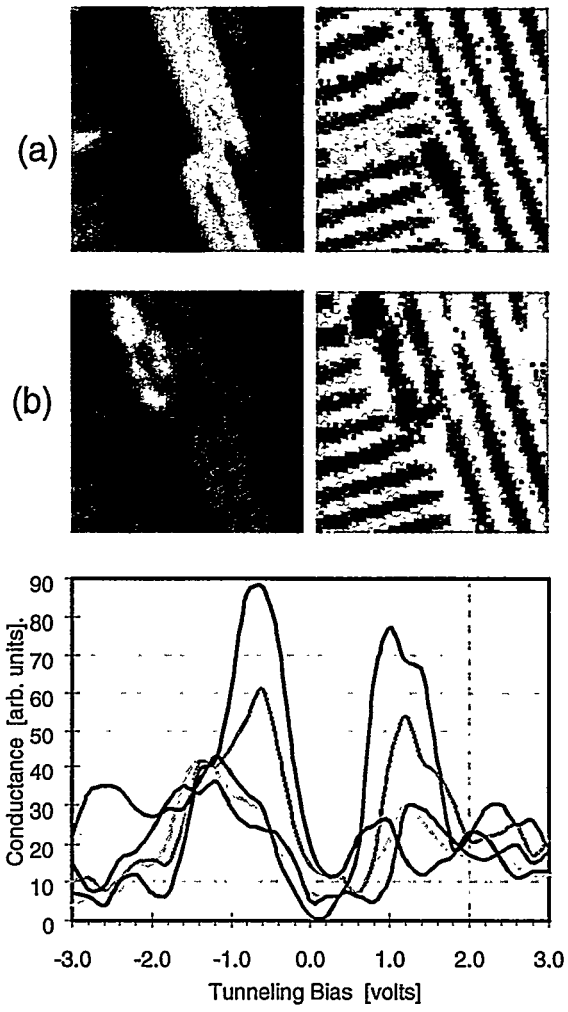

Fig. 7 A-step: Topographic and classed, conductance-based images of kinks in the A-step of a Si(001)-2x1 surface. Common class colors are used in both classed images. Representative conductance spectra of each color-coded, conductance class are shown in the lower plot.

The images in figure 7 were measured using the same STM tip during the same experiment session. Conductance spectra measured from similar features in different regions of the surface are seen to be consistent and reproducible. The tip preparation recipe that is described in the earlier in this report emphasizes tip stability over resolution. In spite of repeated ±3V swings in tip-sample bias during the measurements, spectra from a given tip are consistent. However, we do not yet control the structure of the STM tip sufficiently to achieve reproducible conductance spectra from similar features measured with different tips.

F. Example: B-Step of Si(001) Surface

In the case of the B-step, in which the dimer rows in the upper terrace are perpendicular to the step edge, the classed image reveals several distinct electronic structures along the step. Representative conductance spectra for each class in this example are displayed in figure 8a. A section (outlined in red) of the 75x75 Å topograph shown in figure 8c has been classed and enlarged for display in figure 8b. The corresponding model has been scaled and oriented to the classed image at its lower right.

The classed image contains five classes of conductance. The light and dark gray classes represent the electronic structure of the dimer rows and troughs, respectively; these are labeled A and B, and E and F, in the model. The periodicity of the dimer row structure again agrees with the published model [14]. At the step edge in the classed image, the light gray dimer rows transition abruptly into the blue class of the lower terrace. However, at the termination of the dark gray dimer troughs, a unique, well-localized electronic structure is visible in figure 8b as a cluster of violet pixels at the end of each dimer trough in the upper terrace..

The abrupt termination of the dimer rows in the upper terrace, (corresponding to feature 'E' in the model), is consistent with the fact that the electronic wavefunctions of the dimer bonds can be expected to be

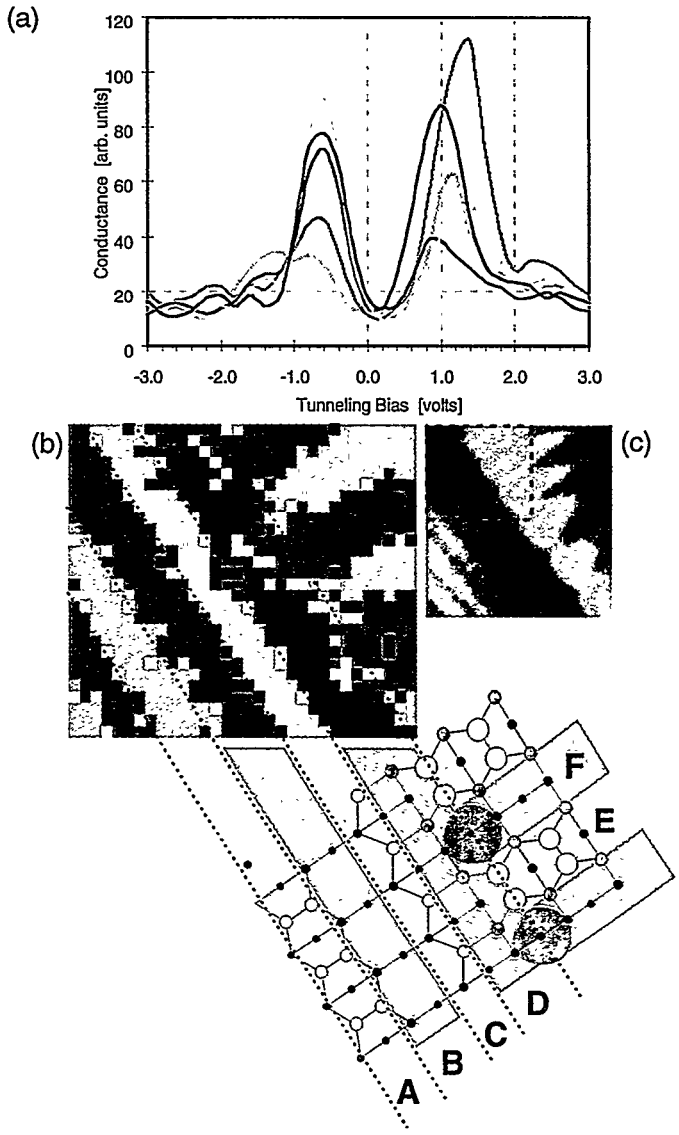

Fig.8 B-step: (a) representative conductance spectra of each color-coded, conductance class, (b) classed image, (c) topographic image - the region outlined in red has been analyzed to generate the classed image. A model of the surface has been scaled and oriented to the classed image at its lower right

much more localized than those of the undimerized, 'dangling' bonds. The fact that the violet class occurs only at the end of the dimer troughs (feature 'F' in the model) may suggest that the dangling bonds which would otherwise 'tie together' dimers along the same row, have been imaged here in the absence of these surrounding dimers.

On the lower terrace, at the base of the B-step, two other electronic structures, not suggested by the topograph, are seen in the classed image. In the region of transition extending from the dimer row structure of the lower terrace ('A' and 'B' of the model) to the step edge, two distinct rows of differing conductance are seen, ('C' and 'D' in the model). The existence of these two electronic structures is fully supported by examination of the conductance spectra displayed in figure 8a. The differences between the spectra of the blue and yellow classes of the step region, and the light and dark gray classes of the terrace, are most obvious at the bias of -0.6V where the measured conductance of the two pairs of classes differ by almost a factor of 2. Within the step region, the spectra of the blue and yellow classes are resolved most distinctly at positive tip-sample biases where the conductance peak of the blue class occurs approximately 0.6V lower than that of the yellow class.

The existence of the electronic structures depicted in the classed image is supported by both the localization of these classes in the real space image and by the uniqueness of their respective conductance spectra. The position of the two classes with respect to the step edge corresponds well with the region of "rebonded" atoms in the model of the single B-step proposed by Chadi [14].

G. Example: 2+1 Vacancy & C-defect on Si(001) Surface

As demonstrated in the previous examples, conductance-based images can discriminate between features whose appearance is indistinct or misleading in a topographic image. A more pointed example of this is displayed in figure 9. In this 150x150 Å scan, a feature is observed that topographically resembles several nearby 2+1 vacancies, but in the conductance-based image, exhibits the electronic properties of a c-defect.

The topographic image shown in figure 9a was recorded just prior to a multispectral conductance measurement of the same region; this 'preview' image was measured with a tip-sample bias of +2.0V and required approximately three seconds to collect. The topograph shown in figure 9b was measured concurrently with the conductance data, also at +2.0V; it required approximately six minutes to collect.

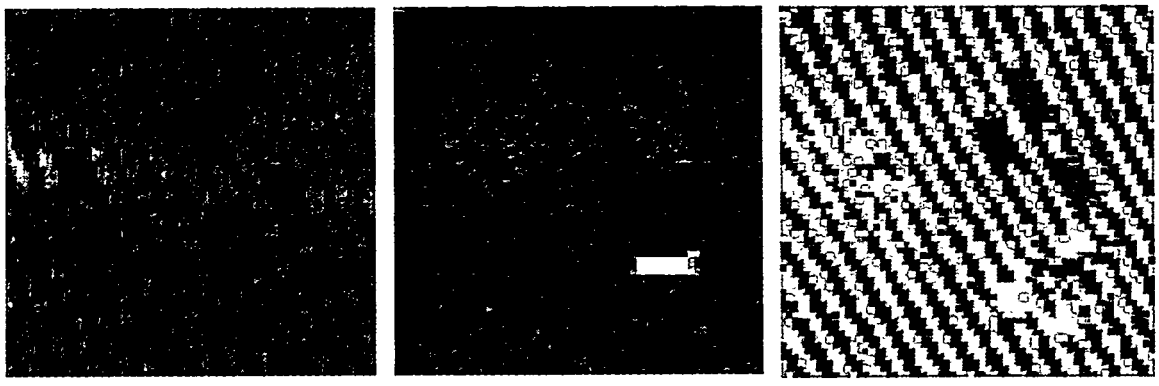

(a) (b) (c)

Fig. 9 2+1 Vacancy & C-defect: (a) +2V topograph recorded in 3 seconds just prior to conductance measurements, (b) +2V topograph recorded concurrently with conductance measurements over a 6 minute period, (c) classed image.

Figure 9c is the false-color classed image resulting from the multispectral image analysis of the conductance data.

As stated previously, images produced from the prolonged, multispectral conductance measurements can exhibit distortions due to uncompensated drift during the measurement; the fast, 'preview' topograph is generally immune to this. The difference in the angle of the dimer rows in figures 9a and 9b is evidence of uncompensated drift. By recording a fast 'preview' topograph just prior to the full multispectral measurement, the presence of this drift is documented and then used in the interpretation of the classed image. It is important to note that because a full conductance spectrum and topographic measurement are recorded at each position of the scan, before proceeding to the next location, the occurrence of a small drift during the multispectral measurement does not affect the accuracy of the measured conductance spectra on which the classification relies. The complete spectral measurement at each pixel requires less than 90 milliseconds, and any slow, long term drift is effectively 'frozen out' during each pixel's multispectral conductance measurement.

A second notable difference between the two topographic images in figure 9 is the presence of a very high-contrast feature in 9b. In the corresponding classed image, this feature is shown in red. Conductance spectra sampled from this feature prove to be consistent across each scan line and are well within the limits of the measurement electronics. Since the feature's conductance at +2.0V is no greater than that measured elsewhere in this surface, the necessity to retract the tip as it scanned over this feature indicates that it is on, rather than in, the surface. Moreover, because the registry of the underlying dimer row structure does not change in the image after the feature is first encountered, and since the measured conductance spectra and tunneling current across the feature in the three ensuing horizontal scan lines remain consistent, it is concluded that the red feature is a metastable adsorbate originating from a non-tunneling portion of the STM tip. We further note that because the topographic image is not used in generating the classed image, it remains an independent comparison of the scanned surface.

The classed image, shown in figure 9c, was computed using conductance images at the biases of +0.6V, +1.6V, and +2.8V; these correspond to 20^{th}, 25^{th}, and 31^{st} panels in figure 10 counting from left to right and top to bottom. A total of six separate conductance classes are detected in the surface.

The dimer rows are again rendered as light and dark gray pixels, respectively. The conductance class

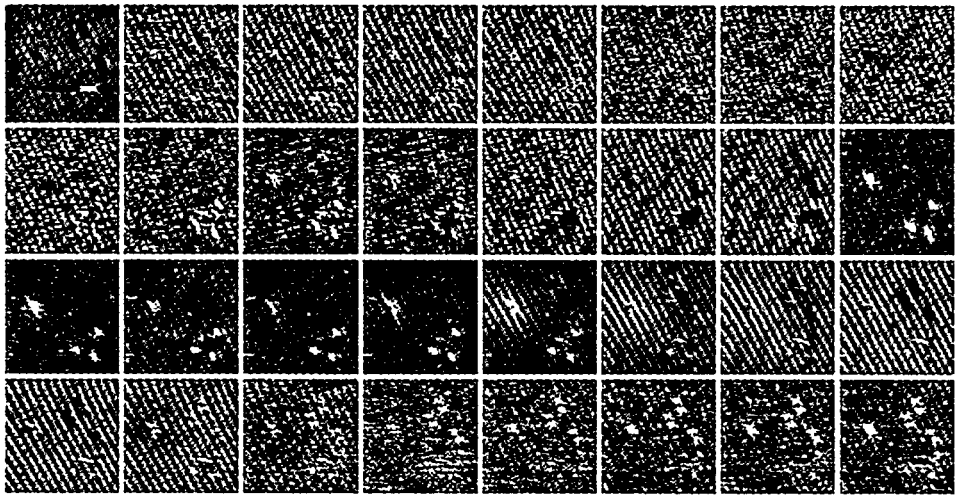

Figure 10. Multispectral conductance images used in the image classification of fig. 9.

corresponding to the 2+1 vacancies is rendered in green. The cluster of c-defects in the lower right consist predominantly of the yellow class, but do exhibit the presence of a small cluster of blue-class pixels. The vacancy-like feature to the left of the 2+1 vacancies corresponds spatially with the outlines of the blue-class at that location in the classed image, though pixels of the yellow conductance class bracket this feature.

Since the classed image is so counter to the suggestion of the topographic image, we present in detail, the spectroscopic data which support the classification. The full set of raw, multispectral, conductance images, which are the sole input to the image classification algorithm, are rendered as an array of 32 images in figure 10. The panel in the upper left is the line-stripped, topographic image recorded at +2.0V. Each subsequent panel, from left to right, displays the intensity of the tunneling conductance measured at successively higher tip-sample biases, over the range -3V to +3V. The conductance data is measured with 12-bit resolution and then scaled into 0-255 gray scale images; brighter pixels represent higher conductance. The presence of distinct features within the various conductance images is easily seen.

The clustering which occurs in the mathematical classification space in this example is portrayed in figure 11. This mathematical space is defined by a y-axis that represents the digitized conductance at a tip-sample bias of +2.8V and an x-axis that represents the conductance measured at +0.6V. A third dimension of +1.6V (not shown) serves to separate the red and green classes from the light gray class. In this plot, each pixel is color-coded according to the results of the computed grouping algorithm's analysis using all three biases.

H. Conclusion

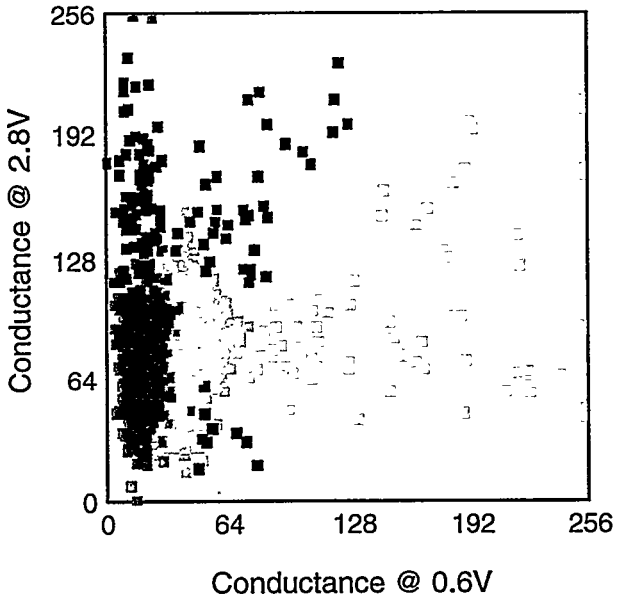

Figure 11. Two-dimensional projection of the mathematical, classification space used to group the pixels in fig. 3c. Each pixel is color-coded according to its assigned class. A third dimension (bias) was used to resolve the overlap of the red and green classes with the gray classes

Comparison of topographic and conductance-based images has shown that surface irregularities in a topographic image do not necessarily indicate the presence of unique electronic structures. Conversely, features which appear topographically similar can in fact exhibit distinctly different electronic behavior. The use of multispectral image analysis techniques in the reduction of multibias STM conductance data provides a quantitative means of examining atomic surfaces, while still maintaining the rich information content inherent in an imaging technique. The use of a computed grouping algorithm greatly streamlines the data reduction process, and provides a rigorous, reproducible means of discriminating features based upon their conductance spectra.

The data presented in this paper were measured with a single STM tip. Multibias conductance images measured with other tips and analyzed with this multivariate classification technique have consistently produced classed images which discriminate between different chemical species and even different bonding states of the same species. However, the exact shape of the conductance spectra defining a specific surface feature differ between tips. This is predominantly due to the variability in both the atom configuration and composition (silicon and tungsten atoms) on the tip side of the tunneling junction. Thus, at present, our classed images only discriminate between surface electronic features, but do not identify them absolutely. We believe that the ability to absolutely identify atoms based upon their conductance spectra can be achieved through strict control or characterization of the STM tip, so that reproducible conductance spectra are measured from surface to surface. This may require utilizing field ion microscopy of the tip before multibias measurements. However, it may also be possible to devise post-measurement transformations of the measured conductance spectra that will factor out variations in tip structure. This latter approach holds some promise since such data transformation techniques are already used in other multivariate classification analyses, e.g. chemical sensing, where similar problems with variability of sensor response and uneven signal attenuation is compensated for by sensor re-calibration and re-normalization of sensor response.

Using a single STM tip, classed images of simple features in Si(001)-2x1 surfaces have been shown to correlate well with obvious features suggested by the corresponding topographic images. The periodicity of the 2x1 dimer row structure, A- and B-step edges, kinks in step edges, 2+1 vacancies and c-defects have all been resolved in conductance-based images of this atomic surface. The classed, conductance-based images have also revealed surface electronic structures not suggested by the topographic images. Classed images of the B-step in the Si(001)-2x1 surface indicate the presence of two electronically distinct rows at the base of the B-step; these features correlate well with the position of "rebonded" atoms proposed in models of the single B-step. Furthermore, the termination of the dimer trough of the upper terrace at the B-step is seen to exhibit unique conductance characteristics, while the termination of the dimer row does not. This may reflect the presence of exposed, undimerized dangling bonds at the step edge. This interdisciplinary approach to the data analysis of multivariate STM data has proven to add significant value to the interpretation of the images of atomic surfaces.

References

1. Hamers, R.J., Tromp, R.M., Demuth, J.E., Phys. Rev. Lett. 1986, 56 (1972).
2. Stroscio, J.A. and Kaiser, W.J.,Eds.; "Scanning Tunneling Microscopy", (Academic Press: San Diego, 1993), p. 137.
3. Feenstra, R.M., Stroscio, J.A., Fein, A.P., Surf. Sci., 181, 295 (1987).
4. Bouchard, A.M., Osbourn, G.C., Swartzentruber, B.S., Surf. Sci., 321, 276 (1994).
5. Stroscio, J.A. and Kaiser, W.J.,Eds.; "Scanning Tunneling Microscopy", (Academic Press: San Diego, 1993), p.,180.
6. Feenstra, R.M., Stroscio, J.A., Fein, A.P., Surf. Sci., 181, 295 (1987).
7. Strocio, J.A. Feenstra, R.M., Fein, A.P. J.Vac. Sci. Technol. A, 5, 838 (1987).
8. Stroscio, J.A., Feenstra, R.M., Newns, D.M., Fein, A.P., J. Vac. Sci. Technol. A, 6, 499 (1988).
9. Martensson, P., Feenstra, R.M. Phys. Rev. B, 39, 7744 (1989).
10. Stroscio, J.A., Feenstra, R.M., Fein, A.P., Phys.Rev. Lett., 57, 2579 (1986).
11. Duda, R.O. and Hart, P.E., "Pattern Classification and Scene Analysis, (John Wiley & Sons, NY, 1973), pp. 66-73.
12. Osbourn, G.C. and Martinez, R.F., Pattern Recognition, , 28, 11, 1793 (1995).
13. http://www.sandia.gov/1100/1155Web/users.htm
14. D.J.Chadi, Phys. Rev. Lett., **59**, 1691 (1987).